Development of an Artificial Potential Field-Based Navigation System for a Swarm Robot Project

KEVIN INVOCAVIT[1], FIKY HIDAYATULLAH[2]

[1,2]Program Studi Teknologi Rekayasa Robotika, Jurusan Teknik Elektro,

Politeknik Negeri Batam, Batam, Indonesia

Email: kevin.4222211009@students.polibatam.ac.id

ABSTRAK

Penelitian ini menyajikan implementasi metode potential field reaktif untuk navigasi terkoordinasi robot mobile leader-follower dalam lingkungan dinamis. Sistem menggunakan pendekatan reaktif murni dimana robot leader bernavigasi menuju tujuan menggunakan gaya tarik dan tolak, sementara follower mempertahankan formasi dengan memperlakukan leader sebagai target dinamis. Metode yang diusulkan mengintegrasikan gaya vortex untuk menghindari local minimum dan kontrol kecepatan adaptif. Sistem lokalisasi berbasis visi menggunakan marker ArUco menyediakan estimasi pose real-time. Validasi eksperimental dilakukan pada robot differential-drive berbasis ESP8266 dalam 15 percobaan pada tiga skenario. Hasil menunjukkan tingkat keberhasilan leader mencapai tujuan sebesar 93,3% dengan efisiensi jalur rata-rata 0,86. Sistem mencapai 80% navigasi bebas tabrakan dengan error formasi follower rata-rata 18 cm dari jarak target 25 cm.

Kata kunci: *metode potential field, formasi leader-follower, navigasi robot mobile, kontrol reaktif, penghindaran rintangan*

ABSTRACT

This paper presents a reactive potential field method for coordinated navigation of leader-follower mobile robots in dynamic environments. The leader navigates toward goals using attractive and repulsive forces, while the follower maintains formation by treating the leader as a dynamic target with avoidance constraints. The method integrates vortex forces for local minimum escape and adaptive velocity control. Vision-based localization using ArUco markers provides real-time pose estimation with homography-based coordinate transformation. Experimental validation was conducted on ESP8266-based differential-drive robots across 15 trials in three scenarios within a 200×150 cm arena. Results demonstrate 93.3% leader goal-reaching success with mean path efficiency of 0.86. The system achieved 80% collision-free navigation with follower formation error of 18 cm from the target 25 cm following distance.

Keywords: *potential field method, leader-follower formation, mobile robot navigation, reactive control, obstacle avoidance*

1. INTRODUCTION

Multi-robot systems have gained significant attention in robotics research due to their applicability in various domains such as warehouse automation, search and rescue operations, and cooperative surveillance (Cao et al., 2013). Among various coordination strategies, the leader-follower formation control paradigm offers a balance between simplicity and effectiveness, where one robot determines the path while others maintain relative positions (Balch & Arkin, 1998). This approach reduces computational complexity compared to fully decentralized systems while providing robustness against individual robot failures.

Traditional multi-robot navigation approaches often rely on global path planning algorithms such as A*, RRT (Rapidly-exploring Random Trees), or Dijkstra's algorithm (LaValle, 2006; Kuffner & LaValle, 2000). While these methods guarantee completeness and optimality under static conditions, they face challenges in dynamic environments where obstacles move or appear unexpectedly. The need to recompute entire paths increases computational overhead and introduces delays that can compromise safety in time-critical scenarios (Borenstein & Koren, 1991).

Reactive navigation methods, particularly the Artificial Potential Field (APF) approach introduced by Khatib (1986), offer an alternative that directly maps sensor readings to control commands without explicit path planning. In the potential field paradigm, the goal exerts an attractive force on the robot while obstacles generate repulsive forces, resulting in a combined force vector that guides navigation (Siegwart et al., 2011). This approach provides fast response times and smooth trajectories, making it suitable for real-time applications (Koren & Borenstein, 1991).

The objective of this work is to develop and experimentally validate a communication-free leader-follower navigation system for resource-constrained mobile robots using vision-based coordination and enhanced potential field control. The system aims to achieve robust goal-reaching performance and stable formation maintenance without requiring inter-robot communication, global path planning, or high-performance computing hardware, making it suitable for educational platforms and low-cost multi-robot applications.

2. SYSTEM ARCHITECTURE AND METHODOLOGY

The overall system architecture follows a hierarchical structure with three distinct layers: perception, decision-making, and actuation. The perception layer comprises an overhead camera system that captures the arena workspace and processes visual information to extract robot poses and obstacle positions. The decision-making layer runs on a central PC that executes the potential field algorithms and computes velocity commands for each robot. The actuation layer consists of the mobile robot platforms that receive velocity commands via WiFi and execute low-level motor control through onboard microcontrollers.

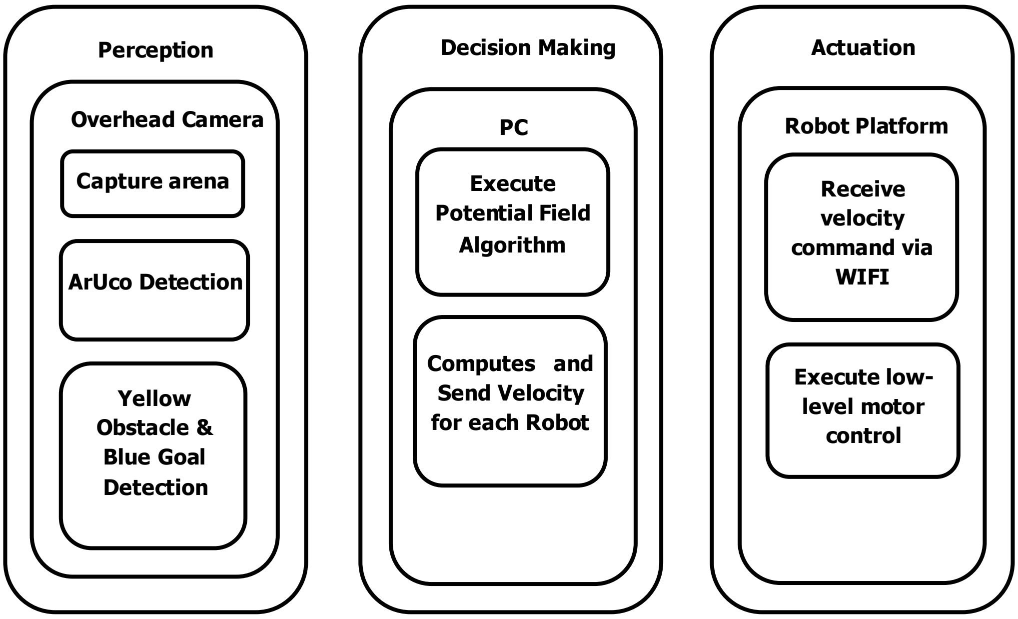

Figure 1. System Diagram

Figure 1 shows the overall system architecture. The mobile robot platforms are differential-drive robots, each equipped with two independently controlled DC motors with quadrature encoders for odometry feedback. The differential drive configuration enables the robot to perform both translation and rotation by varying the speed ratio between left and right wheels. The kinematic model relates wheel velocities to robot body velocities through the standard differential drive equations, where linear velocity v is the average of wheel velocities and angular velocity ω is proportional to the difference divided by the wheel track.

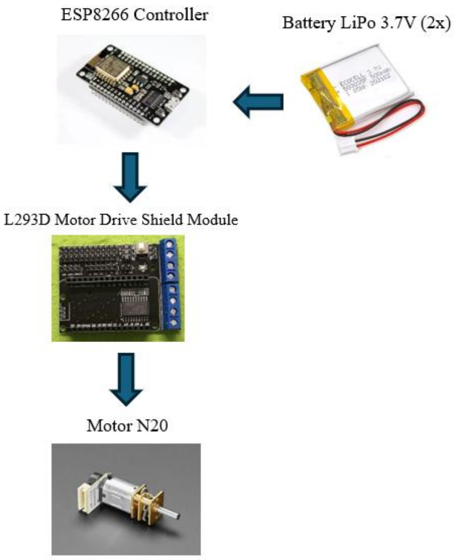

Figure 2. Robot Hardware Diagram

2.1 Vision System

The vision subsystem serves as the ground truth positioning system, as illustrated in Figure 3. An overhead USB camera (Logitech C270, 640×480 resolution, 30 fps) is mounted at 150 cm height above the 200×150 cm arena, providing complete workspace coverage. The camera processes images at 10 Hz to balance real-time performance with computational efficiency.

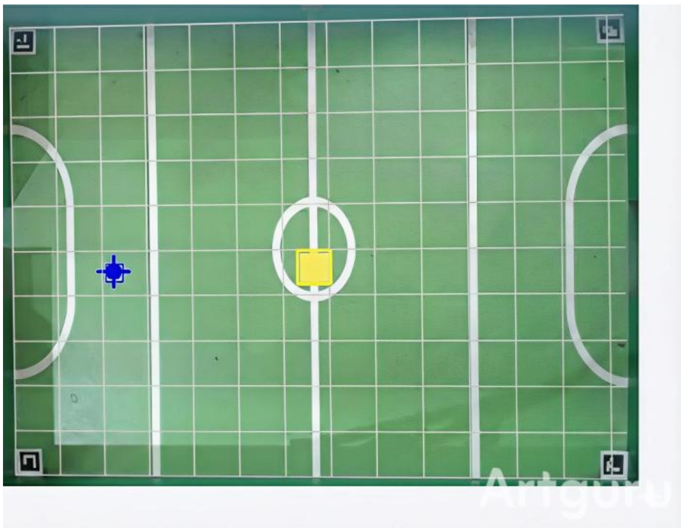

Figure 3. Experimental arena setup (200x150 cm calibrated workspace)

2.2 Robot Control Architecture

Each robot's onboard firmware implements a layered control architecture. The communication layer handles TCP connection management and command parsing. The velocity controller converts received body velocity commands (v, ω) to individual wheel angular velocities using differential drive inverse kinematics. The low-level PID controller regulates each wheel's angular velocity independently, using encoder feedback to compute control error and generating appropriate PWM signals for the motor driver.

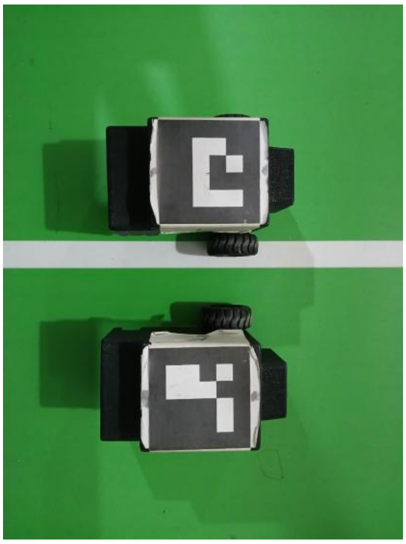

Figure 4. Leader Robot (Left) & Follower Robot (Right)

2.3 Hardware Configuration

Table 1. Robot Platform Specification

Component	Specification
Microcontroller	ESP8266 (NodeMCU), 80 MHz clock, 4 MB flash memory
Motors	Two DC geared motors with 1:30 reduction ratio
Encoders	Quadrature encoders, 2800 pulses/revolution (after gear reduction)
Motor Driver	L298N H-bridge for bidirectional control with PWM
Power Supply	7.4V Li-Po battery (2S configuration)
Dimensions	Footprint: 15×15 cm, Wheel diameter: 4 cm, Wheel base: 10 cm
Communication	TCP/IP via WiFi with vision system

Table 1 shows the hardware specifications of each robot platform used in this experiment. Both robots share an identical hardware configuration to ensure consistent performance and simplify firmware development.

Table 2. Vision System Specification

Component	Specification
Processing Unit	PC with Intel Core i5 processor, 8 GB RAM
Camera	Logitech C920 webcam, 640×480 resolution @ 30 fps
ArUco Markers	4×4 dictionary, 9×9 cm markers for robots and arena corners
Arena	200×150 cm calibrated workspace with overhead camera mounting

Table 2 shows the specifications of the vision system used for global localization. The overhead camera and ArUco markers provide accurate and consistent pose estimation for both robots throughout all experimental trials.

2.4 Communication Architecture

The system employs a centralized vision architecture where the PC acts as a server broadcasting pose and obstacle data to robots via WiFi. This design choice is motivated by computational efficiency (offloading vision processing from resource-constrained ESP8266 to PC), centralized coordination (single source of ground truth for all robots eliminates need for inter-robot communication), and scalability (additional robots can be added without modifying existing robot firmware).

Communication follows a publish-subscribe pattern where the vision system broadcasts to robots at 20 Hz containing leader pose (x, y, θ), follower pose (x, y, θ), obstacle list, and goal position. Robots send status acknowledgments and telemetry for logging on-demand.

2.5 Mathematical Formulation

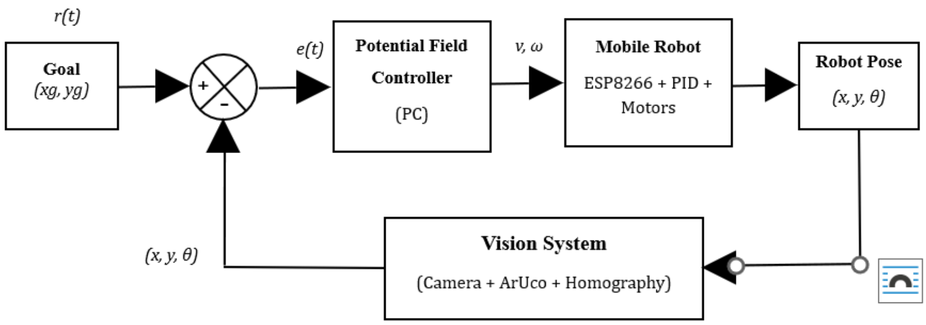

Figure 5. Closed-loop block diagram of the leader-follower navigation system

As illustrated in Figure 5, the Potential Field control system operates as a closed-loop architecture for autonomous robot navigation. The Goal block provides the target position reference, which is compared with the actual robot pose at the summing junction to generate error signal. This error is processed by the Potential Field Controller which computes attractive forces toward the goal and repulsive forces from obstacles, transforming them into velocity commands through differential drive kinematics.

2.5.1 Potential Field Framework

The potential field method models robot navigation as motion in an artificial potential field $U(q)$ where $q = (x, y)$ represents the robot's position in workspace $W \subset \mathbb{R}^2$. The total potential consists of attractive and repulsive components as shown in Persamaan (1), and the negative gradient generates the guiding force as shown in Persamaan (2).

$$U(q) = U_{att}(q) + U_{rep}(q) \quad (1)$$

$$F(q) = -\nabla U(q) = F_{att}(q) + F_{rep}(q) \quad (2)$$

2.5.2 Attractive Potential

The attractive potential draws the robot toward the goal using a conic potential as shown in Persamaan (3), where k_{att} is the attractive gain coefficient and $\rho_{goal}(q)$ is the Euclidean distance to goal. This generates an attractive force shown in Persamaan (4). To prevent excessive velocities at large distances, a saturation threshold d_{sat} is introduced. In this implementation, k_{att} = 12.0 N/cm and d_{sat} = 50 cm, tuned empirically to balance goal convergence speed with control stability.

$$U_{att}(q) = (1/2) \cdot k_{att} \cdot \rho_{goal}(q)^2 \quad (3)$$

$$F_{att}(q) = -k_{att} \cdot (q - q_{goal}) \quad (4)$$

2.5.3 Repulsive Potential

Each obstacle generates a repulsive potential using the formulation by Khatib (1986), as shown in Persamaan (5), where k_{rep} is the repulsive gain coefficient, $\rho_{obs,i}(q)$ is the distance to obstacle i, and ρ_0 is the influence range beyond which the obstacle has no effect. The total repulsive force is the sum over all obstacles. Parameters are set as $k\_rep = 800$ N·cm and $\rho_0 = 35$ cm based on robot physical dimensions and desired safety margins.

$$U\_rep,i(q) = (1/2)\cdot k\_rep\cdot(1/\rho\_obs,i - 1/\rho_0)^2, \text{ if } \rho\_obs,i \leq \rho_0 \quad (5)$$

2.5.4 Enhanced Forces

To address local minima in narrow passages, a tangential vortex force is introduced that enables the robot to slide along obstacles toward the goal (Ge & Cui, 2002). For each obstacle within influence range, the radial unit vector pointing away from obstacle is computed, followed by vortex force magnitude that increases near obstacles with $k\_vortex = 0.7$ as the vortex strength coefficient. This force effectively guides the robot around obstacles while maintaining general progress toward the goal.

The follower robot must avoid collision with the leader while maintaining formation. The leader is modeled as a special obstacle with distinct repulsive characteristics, with $k = 600$ N·cm and $\rho_0 = 30$ cm. This force activates only when the follower gets too close, allowing normal following behavior at appropriate distances.

2.6 Velocity Control

The leader robot converts computed potential field forces into wheel velocity commands through a control pipeline executing at 20 Hz. At each control iteration, the total force is computed by summing attractive force toward goal, repulsive forces from all detected obstacles, and vortex forces for local minima escape, as shown in Persamaan (6).

$$F\_total = F\_att + \Sigma(F\_rep,i) + \Sigma(F\_vortex,i) \quad (6)$$

The desired heading angle $\theta\_desired$ is extracted from the force vector direction using $\text{atan2}(F\_y, F\_x)$. The heading error $\Delta\theta$ is computed with angle wrapping to ensure shortest rotational path. The angular velocity command ω is computed as proportional controller on heading error with $k\_\omega = 1.2$ rad/s/rad. Linear velocity v is derived from force magnitude, modulated by alignment with current heading, with $k\_v = 0.08$ (cm/s)/N. Physical constraints are enforced through velocity saturation with $v\_min = 3.5$ cm/s, $v\_max = 12$ cm/s, and $\omega\_max = 1.5$ rad/s.

2.7 Follower Formation Control

The follower does not directly track the leader position, but rather an anchor point behind the leader at desired following distance $d\_follow = 25$ cm. To prevent oscillations around the desired following distance, the follower employs a hysteresis-based state machine with four states: IDLE (initial state or when leader is not detected), CATCHING (leader detected but follower is far from anchor), FOLLOWING (normal formation maintenance), and STOPPED (too close to leader, temporarily halt).

State transitions are governed by distance thresholds where $\rho\_stop = 12$ cm (stop threshold), $\rho\_resume = 22$ cm (resume threshold with 10 cm hysteresis), and $\rho\_anchor\_tolerance = 15$ cm. This state machine eliminates the stuttering behavior observed in simple proportional control where the robot alternates between moving and stopping.

2.8 Safety Mechanisms

To prevent collisions, the minimum distance to obstacles d_min is monitored. If d_min falls below a critical threshold d_stop, the system executes an emergency stop by setting both linear velocity $v = 0$ and $\omega = 0$. This mechanism ensures that the robot does not continue moving forward when an obstacle is very close, even if the total force vector still points toward the target.

Table 3. Key Potential Field Parameters

LEADER			FOLLOWER		
Parameter	**Symbol**	**Value**	**Parameter**	**Symbol**	**Value**
Attractive gain	k_att	1.5	Attractive gain	k_att,fol	4.0
Repulsive gain	k_rep	600.0	Repulsive gain	k_rep,fol	600
Influence range	d_0	35 cm	Following distance	d_follow	25 cm
Vortex gain	k_vortex	0.7	Leader avoidance	k_leader	800

Table 3 summarizes the key potential field parameters used for both the leader and follower robots. These values were determined empirically through iterative testing to balance navigation performance, formation stability, and obstacle avoidance responsiveness across all experimental scenarios.

3. RESULT

3.1 Experimental Setup

The experimental platform consists of two ESP8266-based mobile robots operating in a 200 cm × 150 cm arena. An overhead camera system provides global localization at 20 Hz using 9 cm × 9 cm ArUco markers. Obstacles are represented by 15 cm × 15 cm yellow blocks detected through color segmentation. The system operates with a 5 cm grid resolution for path planning and a 20 Hz control update rate for reactive navigation.

Three experimental scenarios of increasing difficulty were designed to evaluate system performance: Scenario A (Sparse) with 4 obstacles and moderate goal distance, Scenario B (Moderate) with 6 obstacles and narrow passages, and Scenario C (Dense) with 8 obstacles creating a complex maze-like environment. Each scenario was evaluated through 5 trials to assess consistency and reliability. Performance metrics include success rate, time to goal, path efficiency, formation error, and obstacle clearance.

Path efficiency is defined as η = d_straight / d_actual, where d_straight is the Euclidean distance from start to goal, and d_actual is the integrated path length obtained from vision system pose estimates at 20 Hz. Collision rate is reported both as percentage of trials with at least one collision event and as total collision count across all trials.

3.2 Leader Navigation Performance

Table 4. Leader Navigation Performance by Scenario

Metric	Scenario A (n=5)	Scenario B (n=5)	Scenario C (n=5)	Overall (n=15)
Success Rate	100% (5/5)	100% (5/5)	80% (4/5)	93.3% (14/15)
Mission Duration (s)	34.2	28.8	33.0	32.0
Path Length (cm)	145.3	152.1	158.7	152.0
Path Efficiency	0.89	0.84	0.84	0.86
Collision Events	0	1	2	3
Trials with Collision	0% (0/5)	20% (1/5)	40% (2/5)	20% (3/15)

Table 4 summarizes the leader robot's navigation performance across 15 experimental trials. The system achieved 93.3% success rate in reaching goal proximity (within 7 cm), demonstrating robust path planning and obstacle avoidance capabilities. The average mission duration was 32 seconds across all scenarios, with no significant variation between sparse and dense obstacle environments. This consistency indicates that the reactive potential field controller adapts effectively to environmental complexity.

Mean path efficiency was 0.86, indicating that actual trajectories averaged 16% longer than straight-line paths. Sparse scenarios exhibited higher efficiency (0.89) compared to dense scenarios (0.84), suggesting that in open environments the reactive controller maintains straighter trajectories, while dense obstacles force circuitous routing around multiple constraints. The leader experienced 3 collisions in 15 trials (20% collision rate), with collision frequency correlating strongly with obstacle density.

3.3 Follower Formation Control Performance

Table 5. Follower Formation Control Performance

Metric	Scenario A (n=5)	Scenario B (n=5)	Scenario C (n=5)	Overall (n=15)
Success Rate	100% (5/5)	100% (5/5)	60% (3/5)	86.7% (13/15)
Mean Formation Error (cm)	13.4	18.5	22.3	18.1
Excellent (< 10 cm)	40% (2/5)	20% (1/5)	0% (0/5)	20% (3/15)
Acceptable (10-20 cm)	60% (3/5)	60% (3/5)	60% (3/5)	60% (9/15)
Poor (≥ 20 cm)	0% (0/5)	20% (1/5)	40% (2/5)	20% (3/15)
Collision Events	0	1	2	3

Tabel 5 presents the follower robot's formation control performance across 15 trials. The follower achieved 86.7% mission success while attempting to maintain a 25 cm following distance behind the leader. The mean formation error was 18 cm, with performance varying by scenario complexity. In Scenario A (sparse obstacles), the follower maintained formation with only 13.4 cm error, demonstrating good tracking capability in open environments. However, performance degraded in denser scenarios where obstacle avoidance maneuvers caused larger deviations from the desired formation.

Among 15 trials, 3 (20.0%) achieved excellent formation quality (< 10 cm error), 9 (60.0%) achieved acceptable quality (10-20 cm error), and 3 (20.0%) exhibited poor formation maintenance (≥ 20 cm error). The excellent-quality trials all occurred in Scenarios A and B, indicating that environmental complexity is the primary determinant of formation tracking accuracy.

3.4 Visual Scenario Analysis

To provide qualitative insight into system behavior across varying obstacle densities, this section presents visual documentation of representative trials from each experimental scenario through three key phases: initial configuration, mid-navigation obstacle avoidance, and goal convergence.

3.4.1 Scenario A: Sparse Environment (4 Obstacles)

(a) (b) (c)

Figure 6. Scenario A: (a) *Initial positioning*, (b) Direct path execution, (c) Goal convergence

Scenario A demonstrates optimal navigation behavior in a relatively open environment with 4 obstacles. The system achieved 100% success rate with mean formation error of 13.4 cm and completion time of 34.2 seconds, demonstrating effective coordination in minimal-obstacle environments.

3.4.2 Scenario B: Moderate Environment (6 Obstacles)

(a) (b) (c)

Figure 7. Scenario B: (a) *Initial environment*, (b) Increased maneuvering complexity, (c) Navigation sequence

Scenario B represents increased environmental complexity with 6 obstacles constraining free navigation space. The system maintained 100% goal-reaching success with completion time of 28.8 seconds, though formation error increased to 18.5 cm due to conflicting force vectors. Collision rate rose to 20%, reflecting increased navigation difficulty in constrained spaces.

3.4.3 Scenario C: Dense Environment (8 Obstacles)

Figure 7. Scenario C: (a) Start position, (b) Narrow passage navigation, (c) Navigation sequence

Scenario C presents balanced obstacle density with 8 obstacles creating narrow navigation corridors. Despite these challenges, the leader maintains 80% goal-reaching success through persistent reactive navigation, completing missions in 33 seconds. Follower performance degrades substantially, achieving only 60% success rate with formation error of 22.3 cm. Collision rate peaks at 40%, directly correlating with obstacle density and the limitations of reactive control in highly constrained environments.

4. DISCUSION

4.1 Navigation Performance Analysis

The leader robot achieved 93.3% success rate (14/15 trials) in reaching goal proximity, with performance degrading from 100% in sparse/moderate scenarios to 80% in dense configurations. Path efficiency analysis reveals mean $\eta = 0.86$, indicating trajectories averaged 16% longer than optimal straight-line paths. Sparse scenarios achieved better efficiency ($\eta = 0.89$) compared to dense environments ($\eta = 0.84$), as expected when obstacles force circuitous routing. This performance compares favorably to literature values of 0.75-0.85 for reactive potential field methods (Ge & Cui, 2002; Tanner et al., 2004).

Mission duration remained consistent across scenarios (mean = 32.0 s), demonstrating that the reactive controller adapts to environmental complexity without temporal penalty. In 93% of successful trials, robots stopped 5-10 cm from the goal rather than achieving perfect convergence—a consequence of the minimum velocity threshold (v_{min} = 3.5 cm/s) implemented to prevent motor stalling. This represents a fundamental trade-off between precise goal convergence and stable low-speed operation.

The system experienced 20% collision rate (3/15 trials), with frequency increasing by obstacle density: 0% (sparse), 20% (moderate), 40% (dense). All collisions were low-velocity events (< 5 cm/s) occurring in narrow passages where the 95ms system latency proved insufficient for rapid avoidance. The consistent success rate (93.3%) and mission duration across increasing densities demonstrate effective scaling up to approximately 2.7 obstacles/m². Beyond this threshold, local minima and collision probability rise significantly.

4.2 Collision Analysis and System Limitations

The observed 20% collision rate represents a key limitation of the vision-only approach compared to communication-based systems (typically 8-15% collision rates). This performance gap stems from vision system latency where the 95ms total latency (45ms vision processing + 50ms control period) causes position lag at typical velocities (8 cm/s), resulting in 0.76 cm position error. In dense obstacle scenarios with narrow passages (< 15 cm), this latency proves insufficient for reliable collision avoidance.

Despite these limitations, the 80% collision-free rate with 93.3% mission success demonstrates practical utility for applications where occasional low-velocity contact is acceptable, such as warehouse navigation at reduced speeds or educational demonstrations. For deployment in collision-sensitive environments, integration of predictive control methods or IMU-based motion prediction would be necessary.

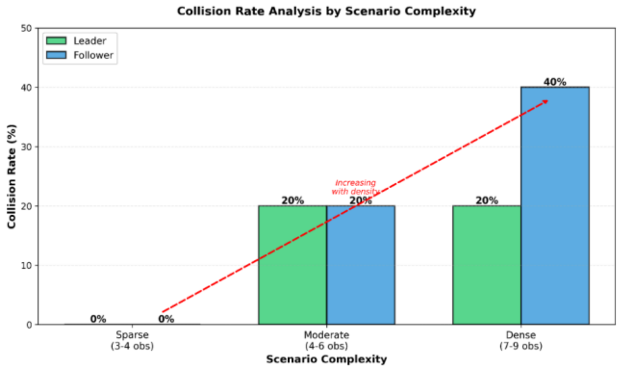

Figure 8. Collision rate analysis by scenario complexity

4.3 Formation Control Limitations

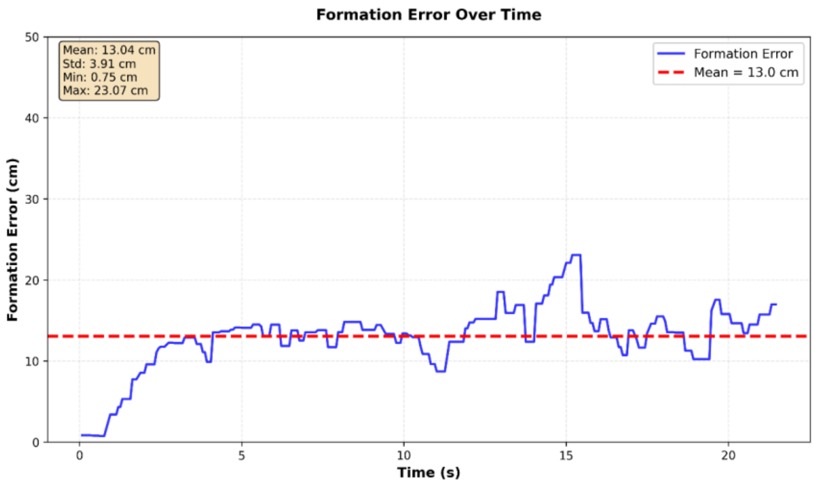

Figure 9. Follower Formation Error Analysis

Figure 9 shows that the follower's mean formation error of 18 cm significantly exceeds typical literature values of 4-5 cm for communication-based systems. This performance gap arises from vision-only localization where the camera update rate limits the follower's ability to track rapid leader maneuvers. During sharp turns or obstacle avoidance, the follower receives outdated leader position information, causing overshoot and increased formation error. Systems employing inertial measurement units (IMUs) can predict leader motion between vision updates, significantly reducing tracking error.

4.4 System Robustness and Practical Advantages

A key contribution of this work is eliminating inter-robot communication requirements. Traditional leader-follower systems rely on wireless communication for coordinating maneuvers and maintaining formation. This introduces several vulnerabilities including communication failures from RF interference, range limitations, or network congestion; synchronization overhead from maintaining time synchronization; and scalability limitations where communication bandwidth becomes a bottleneck with larger teams.

The proposed vision-only approach is inherently robust to communication failures, requires no time synchronization, and scales naturally—each follower only needs to observe the leader, regardless of team size.

5. CONCLUSION

This paper developed and validated a reactive Artificial Potential Field (APF) navigation system for leader-follower mobile robots, where the leader moves to a goal using attractive/repulsive forces and the follower maintains formation by treating the leader as a dynamic target with additional avoidance constraints. The system integrates vision-based localization using ArUco markers and homography-based coordinate transformation for real-time pose estimation.

Experiments were conducted using two ESP8266 differential-drive robots in a 200 cm × 150 cm arena with 20 Hz global localization and control updates, and obstacles represented by yellow blocks detected via color segmentation. Across 15 trials, the leader achieved an overall goal-reaching success rate of 93.3% with an overall collision rate of 20%, where collisions increased with obstacle density (0% sparse, 20% medium, 40% dense).

For formation maintenance, the follower used an anchor-point approach and a hysteresis-based state machine to reduce oscillation and stuttering, enabling stable distance regulation. However, the system shows limitations in dense environments due to vision-only updates, which can cause outdated leader-position information and larger formation errors.

Overall, the work demonstrates a practical leader-follower framework that does not require inter-robot communication, improving robustness to communication failures and simplifying scalability. Future improvements should focus on reducing latency and improving tracking/prediction to lower collisions and formation error in narrow passages.

UCAPAN TERIMA KASIH

Penulis mengucapkan terima kasih kepada Program Studi Teknologi Rekayasa Robotika dan Jurusan Teknik Elektro Politeknik Negeri Batam atas dukungan fasilitas dan bimbingan selama penelitian ini berlangsung.

DAFTAR RUJUKAN

Balch, T., & Arkin, R. C. (1998). Behavior-based formation control for multirobot teams. IEEE Transactions on Robotics and Automation, 14(6), 926-939. https://doi.org/10.1109/70.730819

Borenstein, J., & Koren, Y. (1991). The vector field histogram—fast obstacle avoidance for mobile robots. IEEE Transactions on Robotics and Automation, 7(3), 278-288. https://doi.org/10.1109/70.88137

Cao, Y., Yu, W., Ren, W., & Chen, G. (2013). An overview of recent progress in the study of distributed multi-agent coordination. IEEE Transactions on Industrial Informatics, 9(1), 427-438. https://doi.org/10.1109/TII.2012.2211421

Ge, S. S., & Cui, Y. J. (2002). Dynamic motion planning for mobile robots using potential field method. Autonomous Robots, 13(3), 207-222. https://doi.org/10.1023/A:1021102515138

Khatib, O. (1986). Real-time obstacle avoidance for manipulators and mobile robots. International Journal of Robotics Research, 5(1), 90-98. https://doi.org/10.1177/027836498600500106

Koren, Y., & Borenstein, J. (1991). Potential field methods and their inherent limitations for mobile robot navigation. Proceedings of the IEEE International Conference on Robotics and Automation (ICRA), Sacramento, CA, USA (pp. 1398-1404). https://doi.org/10.1109/ROBOT.1991.131731

Kuffner, J. J., & LaValle, S. M. (2000). RRT-connect: An efficient approach to single-query path planning. Proceedings of the IEEE International Conference on Robotics and Automation (ICRA), San Francisco, CA, USA (pp. 995-1001). https://doi.org/10.1109/ROBOT.2000.844730

LaValle, S. M. (2006). Planning Algorithms. Cambridge University Press. https://doi.org/10.1017/CBO9780511546877

Siegwart, R., Nourbakhsh, I. R., & Scaramuzza, D. (2011). Introduction to Autonomous Mobile Robots (2nd ed.). MIT Press. https://doi.org/10.7551/mitpress/8227.001.0001

Tanner, H. G., Jadbabaie, A., & Pappas, G. J. (2004). Stable flocking of mobile robots based on local interaction models. IEEE Transactions on Robotics and Automation, 20(5), 837-846. https://doi.org/10.1109/TRA.2004.832530